Editors' Suggestion

Surface-Acoustic-Wave Computing of the Grover Quantum Search Algorithm with Metasurfaces

Chenwen Yang,[1] Tuo Liu,[2,3] Jie Zhu,[2,3,*] Jie Ren,[1,†] and Hong Chen[1]

[1] *Center for Phononics and Thermal Energy Science, China-EU Joint Lab on Nanophononics, Shanghai Key Laboratory of Special Artificial Microstructure Materials and Technology, School of Physics Science and Engineering, Tongji University, Shanghai 200092, China*

[2] *The Hong Kong Polytechnic University Shenzhen Research Institute, Shenzhen 518057, China*

[3] *Department of Mechanical Engineering, The Hong Kong Polytechnic University, Hung Hom, Kowloon, Hong Kong SAR, China*

(Received 1 December 2020; revised 31 March 2021; accepted 2 April 2021; published 26 April 2021)

Wave-based computing has attracted extensive attention recently due to the benefits of parallel processing. In particular, several acoustic wave computing devices have been demonstrated to carry out classical algorithms and mathematical operations. Here, we extend acoustic wave computing to simulate a quantum algorithm, by proposing an integrated acoustic gradient metasurface system supporting spoof surface acoustic waves to implement the Grover quantum search algorithm. We show that this integrated metadevice can achieve a designed subdiffraction and transmission phase, which can be used to simulate operations used in a quantum algorithm, such as the Hadamard transformation and the inverse about the average. Numerical simulations demonstrate promising searching abilities of this device, including a quadratic speedup over classical algorithms and subwavelength searching accuracy. We anticipate that our results will inspire alternative design schemes for on-chip integrated metadevices for more quantum-inspired acoustic analog computations.

DOI: 10.1103/PhysRevApplied.15.044040

I. INTRODUCTION

Wave computing, which uses continuously tunable wave quantities to solve calculation problems, has emerged as an alternative computational scheme for signal processing and machine learning [1–3]. Yet, most wave-based computing systems suffer from geometric complexity and diffraction-limited resolution due to the finite wavelength. Recently, a breakthrough in performing mathematical operations with metamaterials [4] has provided wave computing with the opportunity to break these limitations. Metamaterials, composed of artificial units (so-called meta-atoms or metamolecules) arranged in a particular spatiotemporal order, are designed to exhibit exotic properties beyond natural materials.

Along with the use of photonic electromagnetic metamaterials to implement optical wave computing [4], the rapidly expanding research in phononic and acoustic metamaterials [5–12] is enabling people to demonstrate wave analog computing in acoustic subwavelength structures with flexibly tunable effective parameters. For example, it has been shown that by alternating the transmission amplitude and phase of acoustic metamaterials, one can achieve complex mathematical functionalities [13]. These acoustic metastructural systems offer a feasible solution for selective acoustic routing [14,15], acoustic wave analog computing, and signal processing [16–19].

So far, these acoustic wave analog computing systems have carried out only classical algorithms. Quantum algorithms offer an opportunity for us to overcome the limitations of classical algorithms. In order to exploit the efficiency of acoustic metadevice-based wave analog computing, it is interesting to explore a scheme for implementing quantum algorithms with flexible acoustic metamaterials. The Grover search algorithm is among the most significant quantum algorithms [20–22], and provides a powerful method to search a database with quadratic speedup over classical search algorithms. Implementation of the Grover search algorithm has been demonstrated on various quantum systems [23–26]. However, some essential operations of a quantum algorithm, as well as the parallel speedup, may depend solely on the superposition of wave functions, without entanglement [27,28]. Hence, quantum search algorithms can be accomplished by using classical waves, such as in experiments with an optical lens

*jie.zhu@polyu.edu.hk
†Xonics@tongji.edu.cn

system [29] and a microwave system [30], with different polarizations or spatial modes representing the individual quantum states [31].

Unlike bulk metamaterials with unconventional constitutive parameters, metasurfaces are a type of highly engineered flat surface, specifically designed to allow more dynamic and tunable control of waves through sophisticated boundary conditions. Among them, metasurfaces supporting airborne surface acoustic waves (SAWs) [32,33] are capable of serving as a practical, efficient, and flexible way to manipulate acoustic wave propagation at subwavelength scales. The metasurface system that we use in this work uses neatly arranged rectangular resonant cavities with the same cross section [34]. The low geometrical complexity and neat arrangement of these rectangular resonant cavities implies their potential to be integrated on a chip.

In this paper, we show that an acoustic metasurface can be an alternative platform for implementing analog computing of a quantum algorithm with airborne SAWs. We confirm that a gradient-index acoustic system can carry out a Grover search with a quadratic speedup over classical search algorithms. Specifically, we construct an analog-computing metasurface system, composed of different predesigned metasurface boards. We examine the different functions of each of the metasurface boards that perform different operations in the quantum algorithm. When they are put together, we show that the whole metasurface system indeed can carry out the Grover quantum search algorithm. In the foreseeable future, such a SAW-based computing system could offer a flexible platform for wave analog simulation of quantum algorithms, which may potentially find applications in on-chip integrated acoustic and phononic devices.

The paper is organized as follows: In Sec. II, we outline the classical wave-computing scheme for the Grover quantum search algorithm. In Sec. III, we prove that the proposed acoustic system indeed simulates the Grover search algorithm precisely, with a quadratic speedup. Then, in Sec. IV, we construct an airborne-SAW-based Grover-search device utilizing suitably designed acoustic metasurface boards. The simulation results match well with the theory of searching. In Sec. V, finally, we conclude the paper with an extended discussion.

II. GROVER QUANTUM SEARCH ALGORITHM

A binary bit has two basis states, **0** and **1**. A classical bit can be completely described by confirming which basis state it is in, namely whether it is **0** or **1**. A quantum bit (qubit), however, is not simply **0** or **1**, but a superposition of these basis states. In a quantum algorithm, we need a vector to describe a single qubit. Usually, two-element column vectors $\mathbf{0} = \left[\begin{smallmatrix}1\\0\end{smallmatrix}\right], \mathbf{1} = \left[\begin{smallmatrix}0\\1\end{smallmatrix}\right]$ represent the basis states **0** and **1**, and a qubit's state ψ can be represented as $\psi = \alpha\left[\begin{smallmatrix}1\\0\end{smallmatrix}\right] + \beta\left[\begin{smallmatrix}0\\1\end{smallmatrix}\right] = \left[\begin{smallmatrix}\alpha\\\beta\end{smallmatrix}\right]$. α and β are complex numbers representing the amplitudes of the basis states, and must satisfy the requirement $|\alpha|^2 + |\beta|^2 = 1$. Now consider n qubits, each with two basis states. Obviously, the description of an n-qubit system requires us to specify the amplitudes of $N = 2^n$ states. Thus, we need an N-element column vector to describe an n-qubit system.

The Grover quantum search algorithm is made up of three steps before the output [Fig. 1(a)]: an initialize operation, an oracle operation, and an inverse about the average (IAA) [21]:

1. The initialize operation creates a superposition of all N states as the input signal. In order to initialize an equal-superposition state for N computational basis states, the system insert n qubits of **0** state into a Hadamard gate.
2. The oracle operation $\overline{\mathbf{O}}$ contains the information about the position of the target state and marks the target state by reversing the sign of the amplitude. This operation shows a remarkable property of quantum algorithms, known as "quantum parallelism." This means that an operation in a quantum algorithm can operate on all qubits in parallel. Here, $\overline{\mathbf{O}}$ identifies the target state from among N states in a single operation, while a classical sequential algorithm needs N operations to examine all N states one by one. It should be noted that the oracle is a black box that contains the information about the target state. We cannot get information about target states from $\overline{\mathbf{O}}$ directly.
3. The IAA operation is denoted by $\overline{\mathbf{A}}$, and is applied to invert all probability amplitudes about the axis of the average value [20]. The matrix elements of $\overline{\mathbf{A}}$ are defined as

$$A_{ij} = \begin{cases} \dfrac{2}{N}, & i \neq j, \\ -1 + \dfrac{2}{N}, & i = j, \end{cases} \tag{1}$$

which can be rewritten as $\overline{\mathbf{A}} = -\overline{\mathbf{I}} + 2\overline{\mathbf{P}}$. $\overline{\mathbf{I}}$ is the identity matrix, and $\overline{\mathbf{P}}$ is a matrix with elements $P_{ij} = 1/N$ for all i,j. When $\overline{\mathbf{A}}$ acts on an arbitrary vector $\mathbf{V}$, it follows that

$$\overline{\mathbf{A}}\mathbf{V} = -\mathbf{V} + 2\overline{\mathbf{P}}\mathbf{V} = -\mathbf{V} + 2\mathbf{M}, \tag{2}$$

where $\mathbf{M}$ is a mean vector, and $M_i = \sum_{j=1}^{N} P_{ij} V_j = \sum_{j=1}^{N} V_j/N = M$; M_i is the average of all elements of $\mathbf{V}$. Thus, the ith element of $\overline{\mathbf{A}}\mathbf{V}$ is $-V_i + 2M = [M + (M - V_i)]$. Obviously, $\overline{\mathbf{A}}\mathbf{V}$ is the IAA of the vector $\mathbf{V}$.

In a quantum computing system, the IAA operation is usually implemented as $\overline{\mathbf{A}} = \overline{\mathbf{H}}\overline{\mathbf{R}}\overline{\mathbf{H}}$ [21], where $\overline{\mathbf{H}}$ is a Hadamard transform and $\overline{\mathbf{R}}$ is a phase-inversion transform. The IAA is the core operation in the Grover search,

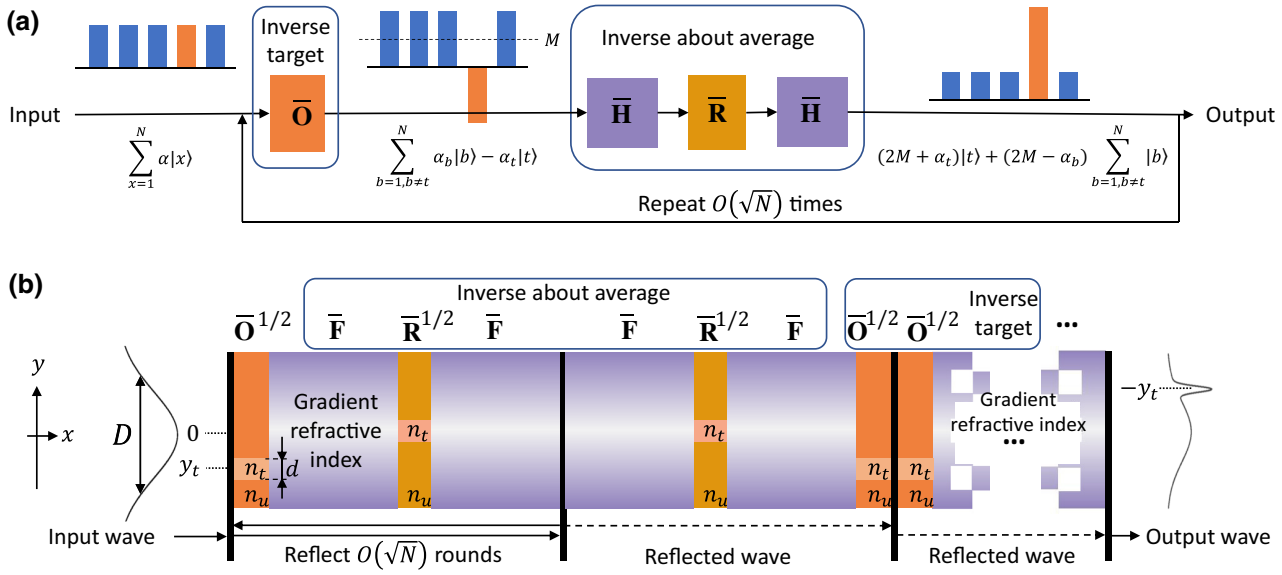

FIG. 1. Diagram of Grover search algorithm in quantum and classical wave systems. (a) Evolution of relative amplitude of quantum states. $\overline{\mathbf{O}}$, $\overline{\mathbf{H}}$, and $\overline{\mathbf{R}}$ represent an oracle operation, a Hadamard transform, and a phase-inversion transform, respectively. The input signal is an equal superposition of all states. The amplitudes of these states are $\alpha = 1/N$. $\overline{\mathbf{O}}$ marks the target state $|t\rangle$ and inverts the target amplitude from α_t to $-\alpha_t$. The IAA performs an inversion of all state amplitudes about the mean, M. Hence, the amplitude of the target state is amplified to $2M + \alpha_t$. (b) Illustration of Grover quantum searching in a classical wave system. The colored areas represent boards that transmit the wave with a designed refractive index. The structures between hard boundaries (thick black lines) represent half an iteration of a full-step search operation. In order to demonstrate the propagation of the reflected wave, we extend the half-iteration system into an array with the hard boundaries as axes of symmetry. The solid arrows below the boards represent the direction of wave propagation, while the dotted arrows below the boards represent the direction of propagation of the wave reflected by the mirrors. $\overline{\mathbf{O}}$ is implemented by a double $\overline{\mathbf{O}}^{1/2}$ board. The IAA is implemented by the sequence $\overline{\mathbf{F}}\overline{\mathbf{R}}^{1/2}\overline{\mathbf{F}}\overline{\mathbf{F}}\overline{\mathbf{R}}^{1/2}\overline{\mathbf{F}}$. The inverse target is achieved by $\overline{\mathbf{O}}^{1/2}\overline{\mathbf{O}}^{1/2}$. The position of the maximum peak of the output wave is located at $-y_t$. The extra negative sign comes from the spatial-inverse functionality of $\overline{\mathbf{F}}^2$.

after which the amplitude of the target state increases significantly [Fig. 1(a)]. When this IAA operation is implemented repeatedly, the amplitude of the target state periodically achieves the maximum, "1."

A series of searching iterations is performed by repeating $\overline{\mathbf{O}}$ and the IAA. The probability amplitude of the target state is amplified after each round trip. In this search algorithm, the number of round trips is called the iteration order. The relationship between the target-state amplitude α_t and the iteration order r is [35]

$$\alpha_t = \sin[(2r+1)\theta]. \tag{3}$$

Here, $\theta = \arcsin(1/\sqrt{N})$. The maximum probability of finding the target state is $\alpha_t^2 = 1$. When N is much larger than 1, $\theta \approx \sin\theta \approx 1/\sqrt{N}$, and the minimum r required to finish a searching process can be expressed as

$$r_f = \frac{\pi}{4}\sqrt{N} - \frac{1}{2}. \tag{4}$$

Considering that the classic sequential search algorithm requires approximately N iterations to find the target, the Grover quantum search algorithm has a quadratic speedup over the classic algorithm ($r_f \sim \sqrt{N}$).

III. IMPLEMENTATION OF GROVER QUANTUM SEARCH IN WAVE SYSTEM

In a quantum algorithm, n quantum bits represent $N = 2^n$ states, which is known as quantum superposition. This combination of N states can be represented by an N-element column vector, which contains the information about the amplitudes and phases of these states. In a classical wave system, the state of a wave element can also be described in terms of amplitude and phase. Because of the benefits of the low-cross-talk nature of the wave system, N independent wave elements construct a superposition state represented by an N-element vector. Similarly to a quantum transformation system, a classical wave transformation system can also process all wave elements using a single operation. Thus, we can use a classical wave system to implement a quantum algorithm [27,28].

To perform the Grover algorithm in a metasurface, we closely follow the three steps listed above, adapted for SAW manipulations:

1. The initialize operation is directly replaced by an incident Gaussian wave. The full width at half maximum (FWHM) of the input Gaussian wave is D, which indicates the length of the entire database [29,30]. We use the normalized pressure amplitude $P(y)$ of the acoustic wave to represent the probability amplitude. The coordinate y marks the positions of items in the database, corresponding to all possible states, and $y = 0$ denotes the horizontal center of all boards.

2. The oracle operation $\overline{\mathbf{O}}$ is performed by a double $\overline{\mathbf{O}}^{1/2}$ board, which is realized by a mirror reflection of a single $\overline{\mathbf{O}}^{1/2}$ board. The index $n_o(y)$ in the oracle board $\overline{\mathbf{O}}^{1/2}$ is n_t at the target position y_t and n_u in other places. In a real searching process, $\overline{\mathbf{O}}^{1/2}$ is a black box; we do not know y_t unless we accomplish the search. All boards in this integrated acoustic metasurface manipulate acoustic waves by means of an adjustment of the acoustic refractive index $n = c_0/c$, where c is the sound speed in the gradient-index (GRIN) material, and c_0 is the sound speed in air. We set n_t and n_u so that $\omega r_0(n_t - n_u)/c_0 = \pi/2$, where r_0 is the length of the $\overline{\mathbf{O}}^{1/2}$ board, and ω is the frequency of the incident wave. Then, after the incident wave is transmitted through the $\overline{\mathbf{O}}^{1/2}$ board, the wave phase at y_t is delayed by $\pi/2$ compared with the phases at other places. In other words, the target state is reversed by a double $\overline{\mathbf{O}}^{1/2}$ board ($e^{i\pi} = -1$). The width of the n_t area, d, is the length of the target data, while the equivalent width of the incident wave is D. Hence, we can obtain the size of the database as $N = D/d$.

3. The IAA operation is realized by the operation $\overline{\mathbf{FR}}^{1/2}\overline{\mathbf{FFR}}^{1/2}\overline{\mathbf{F}}$, which is achieved by a mirror reflection through the boards $\overline{\mathbf{FR}}^{1/2}\overline{\mathbf{F}}$, as shown in Fig. 1(a). Here, the Fourier-transform board $\overline{\mathbf{F}}$ replaces the $\overline{\mathbf{H}}$ operation used in conventional treatments [20,29,30]. It should be noted that two Fourier transforms perform a spatial inversion according to the relation $\overline{\mathbf{F}}\left\{\overline{\mathbf{F}}[f(y)]\right\} \propto f(-y)$, where $f(y)$ is an arbitrary input function. Because $\overline{\mathbf{R}}$ is symmetric about $y = 0$, $\overline{\mathbf{R}}(\mathbf{v}) = \overline{\mathbf{R}}(-\mathbf{v})$ for an arbitrary vector $\mathbf{v}$. Thus, the sequence for the IAA operation is equal to $\overline{\mathbf{FR}}^{1/2}\overline{\mathbf{FFR}}^{1/2}\overline{\mathbf{F}} = \overline{\mathbf{FRF}}$. The $\overline{\mathbf{F}}$ board is constructed with a gradient-index material with refractive index $n_F(y) = n_0\mathrm{sech}\,(\beta y)$, where β is constant. The $\overline{\mathbf{R}}^{1/2}$ board is a phase plane similar to the $\overline{\mathbf{O}}^{1/2}$ board, except that the center position of the n_t area is fixed at the center, $y = 0$.

If we use two hard boundaries as acoustic mirrors to define a half round trip between them [Fig. 1(b)], the acoustic wave is periodically operated on by the sequence $\overline{\mathbf{O}}^{1/2}\overline{\mathbf{FR}}^{1/2}\overline{\mathbf{FFR}}^{1/2}\overline{\mathbf{FO}}^{1/2}$. In a process of multiple iterations, the sequence can also represented as $\overline{\mathbf{OFRF}}$, i.e., the inverse target followed by the IAA. If this search operation is implemented repeatedly, the wave pressure amplitude at the target position periodically achieves its maximum, as described by Eq. (3). To directly illustrate the entire process, we define all half round trips by using a sequence of structures of the same type along the x axis. Adjacent structures are all mirror-reflection symmetrical about the hard boundaries, as shown in Fig. 1(b).

We simulate the acoustic metasurface with ideal GRIN plates to verify the feasibility of implementing the Grover algorithm with airborne SAWs (Fig. 2). The frequency of the incident wave is 4000 Hz, and the wavelength of airborne sound at this frequency is $\lambda = 85.75$ mm. The measurement operations are carried out at the second hard boundary, which at a different position from that of the input signal. Thus, we get our simulation results at half-integer iteration orders. The input Gaussian wave activates an area of width D in the $\overline{\mathbf{O}}^{1/2}$ board. But, still, reflection at the side boundaries may influence the size of the activated area. We use an absorbing boundary condition to eliminate the resulting extra signal.

The simulated pressure-field distribution during searching of an N-item database is shown in Fig. 2(a). As the ratio D/d can be interpreted as the size of the database, we adjust d to obtain different sizes N of the database. The refractive indices of the $\overline{\mathbf{O}}^{1/2}$ and $\overline{\mathbf{R}}^{1/2}$ boards are set to $n_t = 2.57$ and $n_u = 1.5$, and the refractive indices of the $\overline{\mathbf{F}}$ boards are $n_F(y) = n_0\mathrm{sech}\,(\beta y)$, where $\beta = 8$. In order to minimize reflection across different boards, the acoustic impedances of all boards are equal to each other. Since two Fourier transforms perform a spatial inversion, the coordinates of the measurement result differ from the actual coordinates by a negative sign. The results of three simulations with different sizes of the database are demonstrated in Fig. 2. Because we measure the amplitude at half-integer iteration orders only, the maximum value is observed at a half-integer iteration order. According to Eq. (4), when the size of the database is N, the maximum acoustic pressure amplitude at the target position should be measured at a half-integer r_f' close to r_f. Figures 2(b)–2(d) show that the simulated results are in good agreement with the theoretical analysis.

The size of the database, $N = D/d$, needs a double check, as the difference between r_f and r_f' cannot be ignored. According to Eq. (3), the amplitude of the target state changes as a sine function; this is one of the main properties of the Grover search. This means that the maximum value of the target amplitude appears periodically around the maximum value of the sine function. All of the simulations in Fig. 2 have a clear periodic profile. The second maximum value is obtained in Figs. 2(b) and 2(c) at iteration orders of 5.5 and 6.5, respectively, approximated as $(2m + 1)r_f$ with $m = 1$. This reaffirms that the acoustic metasurface system indeed simulates the Grover quantum search algorithm.

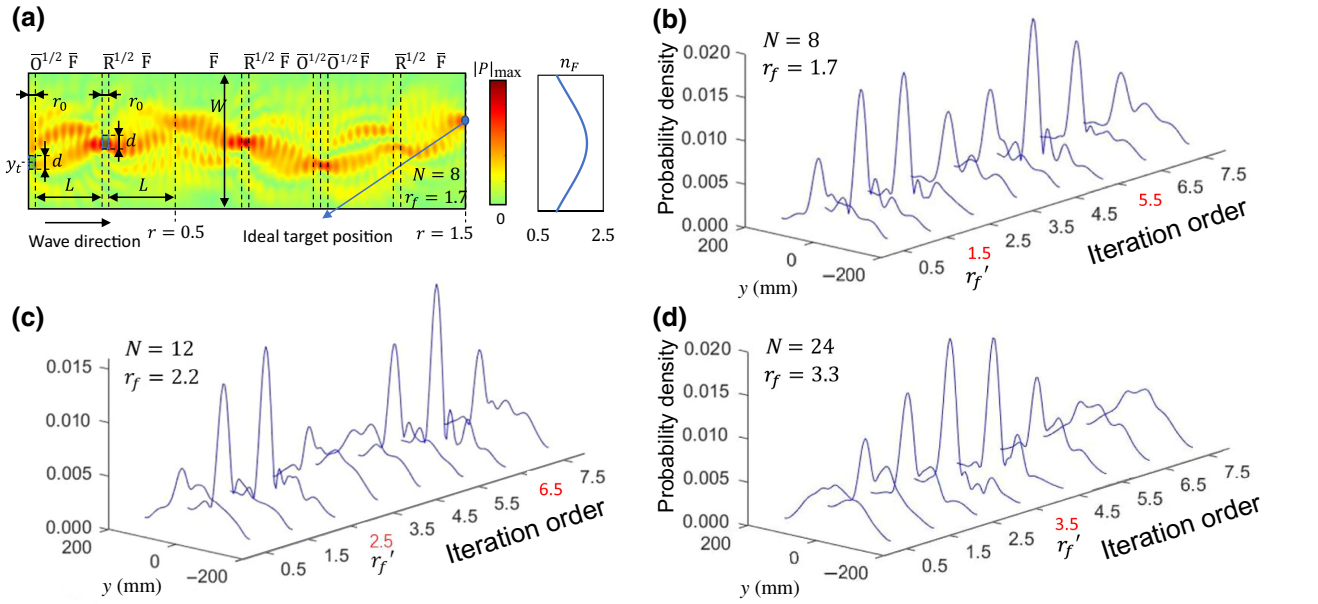

FIG. 2. Simulations with ideal acoustic GRIN distribution. The sound speed in and mass density of the background material are $c_0 = 343$ m/s and $\rho_0 = 1.293$ kg/m^3, respectively. The parameters of the structures are $D = 240$ mm $\approx 2.80\lambda$, $r_0 = 20$ mm $\approx 0.23\lambda$, $W = 310$ mm $\approx 3.61\lambda$, and $y_t = -50$ mm $\approx -0.58\lambda$. We change d to obtain different database sizes N. Here, $n_t = 2.57$ and $n_u = 1.5$. (a) Sound pressure distribution at 1.5 iterations; $d = 30$ mm $\approx 0.35\lambda$. Here, in order to show the details in the y direction more clearly, we increase the y-direction ratio of the image. The ideal target position (blue circle) is marked by $y = 50$ mm $\approx 0.58\lambda$. The right inset shows the refractive index of $\overline{\mathbf{F}}$. (b)–(d) Sound pressure distribution in the direction perpendicular to the propagation direction. The red numbers on the iteration-order axis highlight the maximum-probability iteration order. r_f' denotes the iteration order with the maximum target amplitude in the simulation. We give the theoretical r_f calculated from Eq. (4) in the top left inset.

It should be noted that as d decreases, the FWHM of the main peak at r_f' does not decrease significantly. It is foreseeable that when d is smaller than the FWHM of the main peak, the precise position of the target cannot be obtained from the position of the main peak. This comes from the limitations of the GRIN plate lens. The minimum FWHM at the focal point of the GRIN plate lens is around $0.4\lambda_{\min}$, where $\lambda_{\min}$ is the minimum wavelength inside the GRIN plate lens [36]. Furthermore, the Grover algorithm requires that all wave elements are focused on the center area of the $\overline{\mathbf{R}}^{1/2}$ board, whose width is d. If d is smaller than $0.4\lambda_{\min}$, the center area of the $\overline{\mathbf{R}}^{1/2}$ board will lose some information about the wave elements. Thus, d must be larger than $0.4\lambda_{\min}$.

IV. REALIZATION OF GROVER QUANTUM SEARCH WITH SURFACE ACOUSTIC WAVES

In order to implement the Grover search algorithm with an actual acoustic system rather than an ideal system, we use a gradient metasurface to construct the desired computing device. The effective parameters of metamaterials can be changed precisely by simply adjusting the geometric parameters. In this section, we show that with a metasurface system [34], one can construct an acoustic computing system with a predefined equation for the refractive index and implement the Grover search algorithm precisely.

The acoustic metasurfaces are constructed from a series of neatly arranged square resonators [Fig. 3(a)]. The width, center spacing, and depth of these resonators are denoted by w, a, and h, respectively. The entire structure is immersed in air. A sound wave propagates along the surface with resonators embedded (the x-y plane). Since the impedance of solids is much larger than that of air, we represent the boundary between the air and the frame of the metasurface material as a hard boundary in the simulation.

To achieve a certain effective refractive index, the related h of the square resonators can be calculated from [37]

$$h = \frac{1}{k_0}\arctan \times \left[\frac{1}{k_0}\frac{a^2}{w^2}\left(\sum_{m,n=-\infty}^{+\infty}\frac{\mathrm{sinc}^2(K_m/2)\mathrm{sinc}^2(K_n/2)}{\sqrt{q_{mn}^2 - k_0^2}}\right)^{-1}\right], \tag{5}$$

where $k_0 = \omega/c_0$ denotes the wave number in air for a frequency $f = \omega/2\pi$, and $q_{mn} = \sqrt{{K_m}^2 + {K_n}^2}$ is the

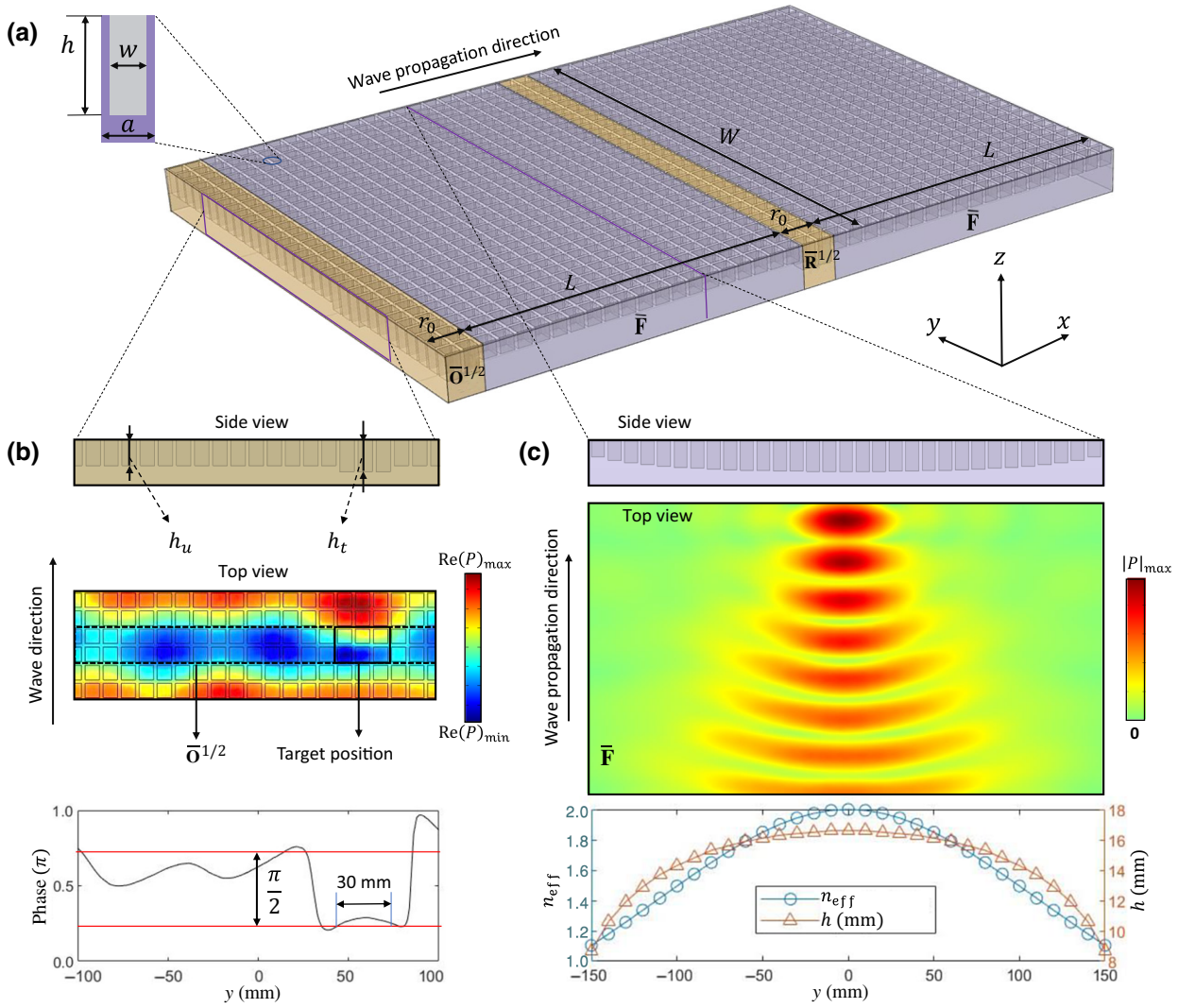

FIG. 3. Illustration of acoustic metasurfaces for the Grover quantum algorithm and its operations. (a) Structure of acoustic metasurface system for emulating Grover search. The left inset is a longitudinal section of a single unit cell; w, a, and h denote the width, center spacing, and depth, respectively, of the resonators. $W = 31a \approx 3.62\lambda$ is the width of the entire structure. The length of the $\overline{\mathbf{F}}$ board is $L = 19a \approx 2.22\lambda$, and the lengths of the $\overline{\mathbf{O}}^{1/2}$ and $\overline{\mathbf{R}}^{1/2}$ boards are both $r_0 = 2a \approx 0.23\lambda$, with $a = 10$ mm $\approx 0.12\lambda$. (b) Illustration of the $\overline{\mathbf{O}}^{1/2}$ board. The top part shows a cross section of the $\overline{\mathbf{O}}^{1/2}$ board between -100 and 100 mm. Here, $h_u = 14.4$ mm $\approx 0.17\lambda$, and $h_t = 17.7$ mm $\approx 0.21\lambda$. The middle part shows the wave propagation in the $\overline{\mathbf{O}}^{1/2}$ board. The dotted black lines highlight the position of the $\overline{\mathbf{O}}^{1/2}$ board. When the acoustic wave propagates above the area where the depth of the target resonator is h_t, the wavelength is shorter than in other areas, so that the wave at the target state has a phase delay compared with those at other places. The bottom part shows the phase of the output wave. (c) Illustration of the $\overline{\mathbf{F}}$ board. The top shows a cross section of the $\overline{\mathbf{F}}$ board. The middle shows the wave pressure distribution in the $\overline{\mathbf{F}}$ board when the board acts on a incident plane wave. The bottom depicts the resonator's depth h and the associated refractive index in the $\overline{\mathbf{F}}$ board.

wave vector of the (m, n)th-order diffracted wave in the plane, where $K_m = (\sqrt{2}/2)n_{\mathrm{eff}}k_0 + (2\pi m/d)$ and $K_n = (\sqrt{2}/2)n_{\mathrm{eff}}k_0 + (2\pi n/d)$. Thus, by controlling the value of h for the square lattice, we can adjust n_{eff} precisely.

Based on Eq. (5), we design a metasurface with an effective refractive-index distribution that is the same as that of the ideal GRIN material presented in Sec. II. In the simulation, we put a line source 10 mm above the metasurface next to the $\overline{\mathbf{O}}^{1/2}$ board to generate the incident airborne SAWs. We set the side length and lattice constant to $w = 8$ mm $\approx 0.94\lambda$ and $a = 10$ mm $\approx 0.12\lambda$, respectively. $W = 31a$ is the width of the entire structure. The length of the $\overline{\mathbf{F}}$ board is $L = 19a$, and the lengths of the $\overline{\mathbf{O}}^{1/2}$ and $\overline{\mathbf{R}}^{1/2}$ boards are $r_0 = 2a$, as shown in Fig. 3(b).

In order to show the properties of the functional boards, we take the $\overline{\mathbf{O}}^{1/2}$ board and $\overline{\mathbf{F}}$ board as examples in Figs. 3(b) and 3(c). In the $\overline{\mathbf{O}}^{1/2}$ board, the surface acoustic wave is delayed at the position of the target data, and the phase difference between the target position and the adjacent position is $\pi/2$. The impedance mismatch and the corresponding interaction between the unit cells may result in unwanted scattering, which consequently leads to an irregular phase variation, as shown in Fig. 3(b). In the Grover algorithm, the "phase-matching" condition requires that the phase delays in the $\overline{\mathbf{O}}^{1/2}$ and $\overline{\mathbf{R}}^{1/2}$ boards must be approximately equal [38], and that the irregular phase delays are much smaller than the phase delay caused by the central area of the $\overline{\mathbf{R}}$ boards. Thus, as long as the measurement is carried out near r_f, we can still get the right position of the target data despite the presence of the unwanted phase variation, as we later verify in simulations of realistic metasurfaces, as shown in Fig. 4. In the $\overline{\mathbf{F}}$ board, the surface acoustic wave converges to the middle at the end of the board. The Fourier transform acts like a focusing lens in a wave system with a predesigned index distribution $n_{\text{eff}}(y)$ [Fig. 3(c)].

The frequency range suitable for the metasurfaces is limited because of the dispersion properties of SAWs [34,37]. When the resonance frequency is approached, anisotropy of the SAWs can be observed, as well as a narrow partial band gap, which leads to direction-dependent wave propagation not applicable to the design of the proposed GRIN metasurfaces. To avoid this, we set the working frequency to 4000 Hz.

According to Fig. 4(a), the maximum peak appears at the position of the target data. Here, the incident wavelength is 85.75 mm, which is much larger than the width of each data point, $3a = 30$ mm. This result clearly shows that the metasurface system can implement the Grover search algorithm with subwavelength accuracy. Conditions with thermal loss are also considered in the simulations, and the positions of the maximum peaks are the same as those with lossless conditions. We also try multiple targets in a single search [Fig. 4(b)]. We set the target positions to -45 and 55 mm, and thus the positions of the target data after searching appear at 45 and -55 mm. We set the size of the targets to $d = 20$ mm $\approx 0.23\lambda$ in the $\overline{\mathbf{O}}^{1/2}$ board, and each target is constructed from two square resonators. The calculation of r_f for multiple targets is the same as in the single-target case, but the size of the database becomes $N = D/(id)$, with i denoting the number of targets. In the original Grover search algorithm for a quantum system,

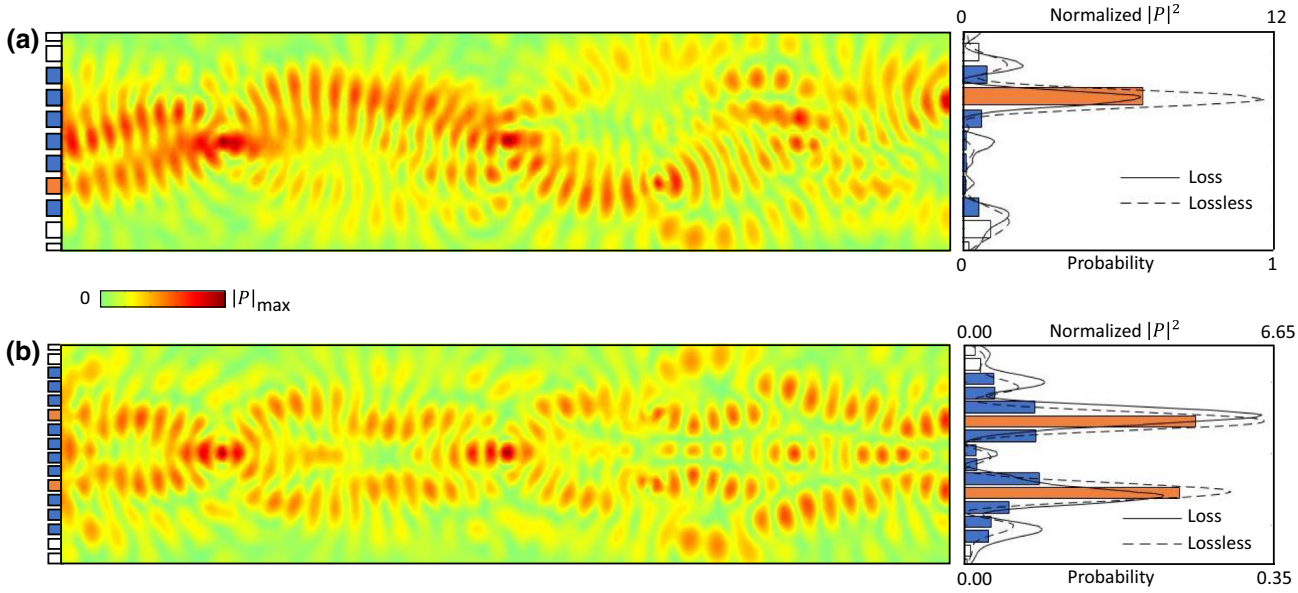

FIG. 4. SAW simulation of Grover search with acoustic metasurfaces. (a) Distribution of wave amplitude (pressure) from position $y = -150$ mm to $y = 150$ mm for an $N = 7$ database. Here, $r_f = 1.52$. The width of each data point is 30 mm. The acoustic wave is fixed precisely at the ideal target position at an iteration order of 1.5. The colored squares at the left show the activated data positions in the $\overline{\mathbf{O}}^{1/2}$ board. The orange square highlights the position of the target data. The white squares denote the inactivated positions. The graph on the right shows the measured results at an iteration order of 1.5. The distribution of the normalized pressure squared (power) is represented by a line graph. The solid line shows the result with thermal loss, and the dotted line shows the result without thermal loss. The maximum acoustic wave amplitude for both loss and lossless conditions appears near the target position. The bar chart describes the probabilities of each data point as targets are searched for with the Grover algorithm. These probabilities are calculated from the distribution of the normalized acoustic pressure squared without thermal loss. (b) Simulation of multiple targets. The width of each data point is 20 mm, while the limit of the GRIN plane is around $0.4\lambda_{\text{min}} = 17.2$ mm.

the probability amplitude of each target state is reduced to $1/i$. After the measurement of the quantum system, we can observe only one of the target states because of the collapse of the wave functions. This influences the efficiency of multiple-target searches. But, there is no collapse of a wave function in classical wave systems. The amplitudes of all wave elements can be measured in a single measurement. All we need is to observe the positions of the maximum peaks. Thus, in a classical wave system, the number of target states does not significantly reduce the success rate of searching.

V. SUMMARY AND DISCUSSION

In summary, we show that an acoustic metasurface system can carry out the Grover search algorithm precisely, based on SAWs. By manipulating wave elements, the acoustic metasurface search system achieves a quadratic speedup over a classical search system. Because of the advantage of the gradient metasurfaces that we use here, subwavelength searching accuracy is obtained in our wave simulation.

One may notice that the amplitude in Fig. 4 has multiple side peaks beside the main peaks. In the Grover search algorithm, the maximum peak of the acoustic wave should appear only at the target position. Actually, the simulations for an ideal material also have multiple side peaks, but they are much smaller than the peaks that we observe for realistic metasurfaces. This is caused by the irregular phase profile in Fig. 3(b) that we mentioned. Also, the metasurfaces are not strictly isotropic and cause an unexpected refractive-index shift. In a quantum system, the wave function can collapse to any possible state, and then one can observe the final state after the collapse. A search process might fail completely because of an impure state. However, in a classical wave system, all we need is to observe the position of the maximum peak. Hence, we can still get the right answer, with the advantage of robustness.

In the work presented in this paper, in order to better present the concept that "quantum algorithms can be implemented with acoustic systems," we choose simple yet reliable square cavities as the building blocks for constructing the GRIN acoustic metasurface. However, due to the limitations of the GRIN system and unwanted scattering, it is difficult to expand the size of the database further. In order to study further the ability of acoustic systems to run quantum algorithms, we need to explore these problems and integrate more design solutions in future. For instance, we may add a scattering-free metasurface [10] to the design of the system in further research to eliminate the influence of unwanted scattering. Or, we could use an elastic GRIN lens [36] to increase further the working frequency and equivalent refractive index of the GRIN plate.

It should be noticed that this searching process is not contrast imaging. The Grover search algorithm can give a periodic amplification profile of the output signal [35], but contrast imaging can not. The periodic behavior of the probability density is a key principle of the Grover algorithm, and we can observe this periodic profile clearly in Fig. 2. In contrast imaging, a clear imaging picture needs a strong source, while the Grover search needs only enough iteration times. The present scheme is fundamentally different from contrast imaging in principle.

We would also like to remark that this acoustic system utilizes mainly the parallel-computing ability of the quantum algorithm rather than quantum entanglement. Considering the flexible nature of acoustic metasurfaces, the Grover algorithm is not the only parallel algorithm that we can implement without real qubits. Given the simple structure, the easy fabrication, and the ability to manipulate waves at subwavelength scales, this flexible structure makes it possible to design various wave analog computing devices. Other extensions of the surface-wave metasystem include the potential for on-chip integration of SAWs in acoustic and phononic devices.

ACKNOWLEDGMENTS

We acknowledge support from the National Natural Science Foundation of China (Grants No. 11935010, No. 11775159, and No. 11774297), the Shanghai Science and Technology Committee (Grants No. 18ZR1442800 and No. 18JC1410900), the Research Grants Council of Hong Kong (Grant No. PolyU 152119/18E), and the Opening Project of the Shanghai Key Laboratory of Special Artificial Microstructure Materials and Technology.

[1] Tyler W. Hughes, Ian A. D. Williamson, Momchil Minkov, and Shanhui Fan, Wave physics as an analog recurrent neural network, Sci. Adv. **5**, eaay6946 (2019).

[2] Farzad Zangeneh-Nejad, Dimitrios L. Sounas, Andrea Alù, and Romain Fleury, Analogue computing with metamaterials, Nat. Rev. Mater. **6**, 207 (2021).

[3] Giulia Marcucci, Davide Pierangeli, and Claudio Conti, Theory of Neuromorphic Computing by Waves: Machine Learning by Rogue Waves, Dispersive Shocks, and Solitons, Phys. Rev. Lett. **125**, 093901 (2020).

[4] Alexandre Silva, Francesco Monticone, Giuseooe Castaldi, Vincenzo Galdi, Andrea Alu, and Nader Engheta, Performing mathematical operations with metamaterials, Science **343**, 160 (2014).

[5] Martin Maldovan, Sound and heat revolutions in phononics, Nature **503**, 209 (2013).

[6] Ming-Hui Lu, Liang Feng, and Yan-Feng Chen, Phononic crystals and acoustic metamaterials, Mater. Today **12**, 34 (2009).

[7] Nianbei Li, Jie Ren, Lei Wang, Gang Zhang, Peter Hänggi, and Baowen Li, Colloquium: Phononics: Manipulating heat

flow with electronic analogs and beyond, Rev. Mod. Phys. **84**, 1045 (2012).
[8] Jensen Li and C. T. Chan, Double-negative acoustic metamaterial, Phys. Rev. E **70**, 055602 (2004).
[9] Steven A. Cummer, Johan Christensen, and Andrea Alù, Controlling sound with acoustic metamaterials, Nat. Rev. Mater. **1**, 16001 (2016).
[10] Junfei Li, Chen Shen, Ana Díaz-Rubio, Sergei A. Tretyakov, and Steven A. Cummer, Systematic design and experimental demonstration of bianisotropic metasurfaces for scattering-free manipulation of acoustic wavefronts, Nat. Commun. **9**, 1342 (2018).
[11] Badreddine Assouar, Bin Liang, Ying Wu, Yong Li, Jian-Chun Cheng, and Yun Jing, Acoustic metasurface, Nat. Rev. Mater. **3**, 460 (2018).
[12] Y. Xie, W. Wang, H. Chen, A. Konneker, B. I. Popa, and S. A. Cummer, Wavefront modulation and subwavelength diffractive acoustics with an acoustic metasurface, Nat. Commun. **5**, 5553 (2014).
[13] Shuyu Zuo, Qi Wei, Ye Tian, Ying Cheng, and Xiaojun Liu, Acoustic analog computing system based on labyrinthine metasurfaces, Sci. Rep. **8**, 10103 (2018).
[14] Yang Long, Danmei Zhang, Chenwen Yang, Jianmin Ge, Hong Chen, and Jie Ren, Realization of acoustic spin transport in metasurface waveguides, Nat. Commum. **11**, 4176 (2020).
[15] Yang Long, Hao Ge, Danmei Zhang, Xiangyuan Xu, Jie Ren, Ming-Hui Lu, Ming Bao, Hong Chen, and Yan-Feng Chen, Symmetry selective directionality in near-field acoustics, Natl. Sci. Rev. **7**, 1024 (2020).
[16] Shuyu Zuo, Qi Wei, Ying Cheng, and Xiaojun Liu, Mathematical operations for acoustic signals based on layered labyrinthine metasurfaces, Appl. Phys. Lett. **110**, 011904 (2017).
[17] ShuYu Zuo, Ye Tian, Qi Wei, Ying Cheng, and Xiaojun Liu, Acoustic analog computing based on a reflective metasurface with decoupled modulation of phase and amplitude, J. Appl. Phys. **123**, 091704 (2018).
[18] Anders Pors, Michael G. Nielsen, and Sergey I. Bozhevolnyi, Analog computing using reflective plasmonic metasurfaces, Nano Lett. **15**, 791 (2015).
[19] Farzad Zangeneh-Nejad and Romain Fleury, Performing mathematical operations using high index acoustic metamaterials, New J. Phys. **20**, 073001 (2018).
[20] Lov K. Grover, in *Proceedings of the Twenty-Eighth Annual ACM Symposium on Theory of Computing* (ACM Press, New York, 1996) p. 212.
[21] Lov K. Grover, Quantum Mechanics Helps in Searching for a Needle in a Haystack, Phys. Rev. Lett. **79**, 325 (1997).
[22] Lov K. Grover, Quantum Computers Can Search Rapidly by Using Almost any Trasformation, Phys. Rev. Lett. **80**, 4329 (1998).
[23] Issac L. Chuang, Neil Gershenfeld, and M. Kubinec, Experimental Implementation of Fast Quantum Searching, Phys. Rev. Lett. **80**, 3408 (1998).
[24] K. A. Brickman, P. C. Haljan, P. J. Lee, M. Acton, L. Deslauriers, and C. Monroe, Implementation of grover's quantum search algorithm in a scalable system, Phys. Rev. A **72**, 050306 (2005).
[25] Klaus Mølmer, Larry Isenhower, and Mark Saffman, Efficient grover search with rydberg blockade, J. Phys. B **44**, 184016 (2011).
[26] Stefanie Barz, Elham Kashefi, Anne Broadbent, Joseph F. Fitzsimons, Anton Zeilinger, and Philip Walther, Demonstration of blind quantum computing, Science **335**, 303 (2012).
[27] Seth Lloyd, Quantum search without entanglement, Phys. Rev. A **61**, 010301(R) (1999).
[28] David A. Meyer, Sophisticated Quantum Search Without Entanglement, Phys. Rev. Lett. **85**, 2014 (2000).
[29] N. Bhattacharya, H. B. van Linden van den Heuvell, and R. J. C. Spreeuw, Implementation of Quantum Search Algorithm Using Classical Fourier Optics, Phys. Rev. Lett. **88**, 137901 (2002).
[30] W. Zhang, K. Cheng, C. Wu, Y. Wang, H. Li, and X. Zhang, Implementing quantum search algorithm with metamaterials, Adv. Mater. **30**, 1703986 (2018).
[31] P. G. Kwiat, J. R. Mitchell, P. D. D. Schwindt, and A. G. White, Grover's search algorithm: An optical approach, J. Mod. Opt. **47**, 257 (2000).
[32] Luc Kelders, Jean F. Allard, and Walter Lauriks, Ultrasonic surface waves above rectangular-groove gratings, J. Acoust. Soc. Am. **103**, 2730 (1998).
[33] Zhaojian He, Han Jia, Chunyin Qiu, Yangtao Ye, Rui Hao, Manzhu Ke, and Zhengyou Liu, Nonleaky surface acoustic waves on a textured rigid surface, Phys. Rev. B **83**, 132101 (2011).
[34] Tuo Liu, Fei Chen, Shanjun Liang, He Gao, and Jie Zhu, Subwavelength Sound Focusing and Imaging Via Gradient Metasurface-Enabled Spoof Surface Acoustic Wave Modulation, Phys. Rev. Appl. **11**, 034061 (2019).
[35] M. Boyer, G. Brassard, P. Hoyer, A. Tapp, M. Boyer, and G. Brassard, Tight bounds on quantum searching, Fortschr. Phys. **46**, 493 (1996).
[36] Jinfeng Zhao, Xiaodong Cui, Bernard Bonello, Bahram Djafari-Rouhani, Weitao Yuan, Yongdong Pan, Jie Ren, Xiaoqing Zhang, and Zheng Zhong, Broadband subdiffraction and ultra-high energy density focusing of elastic waves in planar gradient-index lenses, J. Mech. Phys. Solids **150**, 104357 (2021).
[37] Tuo Liu, Shanjun Liang, Fei Chen, and Jie Zhu, Inherent losses induced absorptive acoustic rainbow trapping with a gradient metasurface, J. Appl. Phys. **123**, 091702 (2018).
[38] Gui Lu Long, Yan Song Li, Wei Lin Zhang, and Li Niu, Phase matching in quantum searching, Phys. Lett. A **262**, 27 (1999).